A Low-Disturbance Nonequilibrium Molecular Dynamics Algorithm Applied to the Determination of Thermal Conductivities

Filipe A. Furtado
Programa de Engenharia Química/COPPE, Universidade Federal do Rio de Janeiro, Cidade Universitária, Rio de Janeiro, 21941-972 RJ, Brazil

Charlles R. A. Abreu
Escola de Química, Universidade Federal do Rio de Janeiro, Cidade Universitária, Rio de Janeiro, 21949-900 RJ, Brazil

Frederico W. Tavares
Programa de Engenharia Química/COPPE, Universidade Federal do Rio de Janeiro, Cidade Universitária, Rio de Janeiro, 21941-972 RJ, Brazil

Escola de Química, Universidade Federal do Rio de Janeiro, Cidade Universitária, Rio de Janeiro, 21949-900 RJ, Brazil

DOI 10.1002/aic.14803
Published online April 3, 2015 in Wiley Online Library (wileyonlinelibrary.com)

A new nonequilibrium molecular dynamics algorithm is proposed for the determination of thermal conductivity and other transport properties. The proposed algorithm aims at diminishing the energy drift problem observed in this type of method while conserving linear momentum and being compatible with constrained molecules. The features of the proposed algorithm are evaluated by determining thermal conductivities of water at 323 K, n-octane at 300 K, and argon close to its triple point, and by comparing these results with those obtained using established methods. The analysis of systems presenting diverse molecular characteristics allowed us to assess the usefulness of the proposed algorithm. The energy drift and temperature variation were reduced in the range of 10–80%, depending on the parameters of the proposed algorithm and the characteristics of the system. The determined thermal conductivities showed good agreement when compared to experimental and simulation data. © 2015 American Institute of Chemical Engineers *AIChE J*, 61: 2881–2890, 2015

Keywords: thermal conductivity, nonequilibrium molecular dynamics, transport properties, energy drift

Introduction

Transport phenomena are continuously studied due to their importance for the development of industrial applications.[1–3] In the oil industry, the availability of reliable transport properties of complex hydrocarbon mixtures would allow a more precise modeling of oil reservoirs.[4–7] In addition, a better understanding of transport processes could offer reasonable explanations to poorly understood natural phenomena, with possible use in the development of biological applications.[8] Nowadays, the continuously growing interest in geological storage of gases such as CO_2 demands transport properties of pure substances and mixtures at extreme conditions, which involves complex experimental setups. Many mathematical models available in the literature are based on empirical correlations, which limits their applicability to the ranges of experimental conditions used to estimate their parameters.[9] In all those circumstances, computational techniques, such as molecular dynamics simulations, can be useful tools for reducing the costs with experimental evaluation of transport properties.[3,9–13]

Along the past years, several molecular simulation methods have been developed for the determination of transport properties, which involve the simulation of systems at equilibrium (equilibrium molecular dynamics, EMD[14–16]) or out of equilibrium (nonequilibrium molecular dynamics, NEMD[17–21] or transient molecular dynamics[22–24]). Transport property determination using EMD is based on the Linear Response Theory.[25–27] Evaluation of the natural decay of correlation functions of microscopic fluxes allows the use of the Green–Kubo formalism[28,29] to obtain several transport properties in a single EMD simulation run.[3] Regardless of this advantage, EMD exhibits some disadvantages such as poor convergence of the time integrals of flux correlation functions and ambiguous definition of the microscopic heat flux for multicomponent systems.[3,20,30,31] Conversely, with NEMD methods the system properties converge more rapidly

Correspondence concerning this article should be addressed to F. W. Tavares at tavares@eq.ufrj.br.

and the heat fluxes are exactly defined for any system, despite the number of components.[19,20,32]

Notwithstanding all the mentioned benefits of molecular dynamics, one must bear in mind that most force fields have been developed to reproduce thermodynamic data. Thus, tests are often required to assess the reliability of an existing force field in reproducing transport properties.[3]

The most common class of NEMD methods is referred to as boundary driven nonequilibrium molecular dynamics (BD-NEMD).[33] It consists in controlling the boundaries of the simulation box to impose a driving force (e.g., a temperature gradient) and a corresponding flux (e.g., heat flux) in the system. In a BD-NEMD simulation, a box with periodic boundary conditions is initially divided into several slabs of equal thickness along one direction. Subsequently, two slabs are chosen so that energy is added to one of them (tagged as the "hot slab") and removed from the other one (tagged as the "cold slab"). For the sake of symmetry, it is important that the distance between the hot and cold slabs (measured from their central planes) is equal to half the box size in the corresponding direction. By periodically performing the described energy addition/removal, a heat flux and temperature gradient will take place between the hot and cold regions. Once steady state is reached, the thermal conductivity can be determined using Fourier's Law.[19,33]

Different procedures may be applied to control the hot and cold regions of the simulation box.[33] Two well-known BD-NEMD methods are the heat exchange algorithm (HeX) developed by Hafskjold et al.[18] and the momentum exchange algorithm (PeX) developed by Müller-Plathe.[19] In the HeX algorithm, the velocities of the atoms contained in the tagged slabs are rescaled so that the same amount of energy removed from the cold slab is added to the hot one. By performing these exchanges periodically, the system will reach the steady state with a defined energy flux and temperature gradient.[18,33] In the PeX algorithm,[19] energy is artificially transferred by swapping the velocities of the slowest atom in the hot slab and the fastest atom in the cold slab. For the total momentum of the system to be conserved, these two atoms must have equal mass. The kinetic energy periodically transferred in such a nonphysical way ultimately flows back to the cold region by physical mechanisms. An important improvement on the PeX algorithm for molecular systems consists in swapping center-of-mass velocities of molecules, thus avoiding deformations.[20] Another improved PeX algorithm is the one devised by Nieto-Draghi and Avalos,[21] in which the momentum exchange is carried out as if the chosen atoms in the cold and hot slabs underwent an elastic collision. This strictly satisfies momentum conservation and thus circumvents the mass equality restriction of the original PeX (in fact, it reduces to the original method when the mass equality holds).

The advantages of the PeX methods are (1) the adherence to conservation laws in their formulations, (2) the natural compatibility with periodic boundary conditions, and (3) the use of Newtonian dynamics in the intermediate slabs. However, the system must be large enough for each slab to behave as a thermodynamic system.[18,19,33–36] Two other drawbacks are generally observed. The first one is that large driving forces (temperature differences) are generally needed between the two-tagged slabs (the measured properties are generally reported at the average temperature of the simulation box). This requires caution to avoid phase transitions, which can occur if the temperatures of the tagged slabs exceed melting and/or boiling points.[33–36] The second drawback is the drift in the total energy of the system caused by the constantly imposed perturbations,[34,35] which increases the average box temperature over time, thus interfering in the determined transport properties. This problem is commonly avoided by weakly coupling a Berendsen thermostat to the system.[34,35] According to Zhang et al.,[35] the differences in thermal conductivities determined with and without the use of a thermostat are around 10%, which was considered not significant. However, given that thermostats act directly on the atomic velocities, they can affect the dynamics of the system and their use should be minimized or avoided. Recently, Kuang and Gezelter[37] developed an algorithm that can potentially alleviate the energy drift problem, but it has not been tested in this context. Atom velocities in the tagged slabs are rescaled in a nonisotropic way while momentum and energy are conserved and a predefined energy flux is imposed. In addition, minimum anisotropy is forced so that up to four scaling parameter sets remain as feasible choices. Then, a least-perturbation criterion is adopted when choosing among these sets. In another article,[38] the authors proposed a simpler algorithm which is capable of specifying thermal and momentum fluxes simultaneously, but has less flexibility with respect to the least-perturbation criterion.

Taking the discussion above into consideration, the goal of this article is to propose a new BD-NEMD algorithm that intrinsically contains a minimum disturbance criterion in its formulation considering both the orientation and magnitude of momentum vectors. In addition, the method developed here can be used to exchange energy between molecules with internal constraints, or among all atoms present in the tagged slabs, provided that the transfer is performed using the translational kinetic energy of the group of atoms in question, such as proposed by Bedrov and Smith.[20] Once the disturbance is small at every transfer event, the system is expected to undergo small energy drift and temperature variation over time. To evaluate the algorithm, the energy and temperature variations are compared to those exhibited by the PeX algorithms of Müller-Plathe (hereafter referred to as MP) and of Nieto-Draghi and Avalos (referred to as ND&A). The three BD-NEMD algorithms (MP, ND&A, and the one proposed here) are used to simulate *n*-octane at 300 K, water at 323 K, and argon close to its triple point. For *n*-octane, the Nath, Escobedo and de Pablo Revised force field (NERD)[39] and Optimized Potentials for Liquid Simulations (OPLS-UA flex)[40–42] force fields were used to evaluate the influence of bond stiffness (the latter corresponds to the OPLS-UA force field augmented with flexible bonds and angles). The influence of time step size was also evaluated using OPLS-UA flex. Water was modeled using the SPC/Fw[43] force field to evaluate the behavior of the proposed algorithm in systems with electrostatic interactions. Argon was modeled using the Lennard-Jones potential to evaluate the energy drift when internal degrees of freedom are not present. The thermal conductivities obtained using the different BD-NEMD algorithms were compared with reference results found in the literature.

Proposed Algorithm

After an energy transfer event occurs using one of the well-established PeX algorithms (e.g., MP or ND&A), the velocities of the involved atoms change instantaneously in both direction and magnitude, thus causing a disturbance in

the Newtonian dynamics.[44] In this way, excessive bond stretching, angle bending, or atom overlapping can occur in the subsequent steps. Together with round-off and cutoff errors,[35] this fact eventually leads to the artificial energy increase commonly observed in these nonequilibrium simulations. Following this reasoning, if it is possible to chose new velocity vectors which are very similar to the old ones, while still promoting the desired energy transfer and conserving total energy and linear momentum, one expects that the energy drift problem is reduced.

The goal of the proposed algorithm is to transfer a predefined amount of energy between two particles at a given time step, causing the smallest possible perturbation to the system. Note that what we call a particle can in fact be an atom, a molecule, or even a group of unconnected atoms/molecules, given that the total linear momentum and translational kinetic energy of the group of atoms are employed in the calculations. After the transfer event, even though the center-of-mass velocity of a group of particles changes, the relative velocities of its atoms are kept constant.[20]

Consider that a specified amount of energy ΔE is to be transferred from a particle i, whose mass is m_i, to a particle j, whose mass is m_j. Before the transfer is performed, the linear momentum vectors of these particles are $\mathbf{p}_i^0$ and $\mathbf{p}_j^0$, respectively, and the total momentum of the pair is $\mathbf{p}=\mathbf{p}_i^0+\mathbf{p}_j^0$. In the same situation, the kinetic energies of particles i and j are, respectively

$$E_i^0=\frac{\|\mathbf{p}_i^0\|^2}{2m_i} \quad \text{and} \quad E_j^0=\frac{\|\mathbf{p}_j^0\|^2}{2m_j} \tag{1}$$

Because the particles must remain in the same positions, only kinetic energy can be transferred. Of course, the amount ΔE is limited by the initial kinetic energy of particle i, that is, $\Delta E \leq E_i^0$. After the transfer, particles i and j will have new linear momenta $\mathbf{p}_i$ and $\mathbf{p}_j$, but the total momentum and the total kinetic energy of the pair must be kept unaltered. These conditions are expressed as

$$\mathbf{p}_j+\mathbf{p}_j=\mathbf{p} \tag{2}$$

$$p_{ix}^2+p_{iy}^2+p_{iz}^2=2m_i(E_i^0-\Delta E) \quad \text{and} \tag{3}$$

$$p_{jx}^2+p_{jy}^2+p_{jz}^2=2m_j(E_j^0+\Delta E) \tag{4}$$

where the subscripts x, y, and z denote the components of the momentum vectors. This provides five equations relating six unknowns, which are the components of vectors $\mathbf{p}_i$ and $\mathbf{p}_j$. The sixth equation necessary for obtaining these components will be introduced later on. By defining new variables $R_i^2=2m_i(E_i^0-\Delta E)$ and $R_j^2=2m_j(E_j^0+\Delta E)$ and substituting Eq. 2 into Eq. 4, we obtain

$$p_{ix}^2+p_{iy}^2+p_{iz}^2=R_i^2 \quad \text{and} \tag{5}$$

$$(p_{ix}-p_x)^2+(p_{iy}-p_y)^2+(p_{iz}-p_z)^2=R_j^2 \tag{6}$$

Note that, in the space of possible linear momentum vectors of particle i, Eq. 5 represents a sphere with radius R_i centered at the origin and Eq. 6 represents a sphere with radius R_j centered at (p_x, p_y, p_z). Therefore, after carrying out the energy transfer, the momentum of particle i must lie in the intersection circumference between these two spheres. This is illustrated in Figure 1, where the red sphere comes from Eq. 5 and the yellow sphere comes from Eq. 6. The locus of all momenta $\mathbf{p}_i$ that preserve the total momentum and the total kinetic energy is drawn as a black circumference. One of these momenta was arbitrarily chosen and depicted in Figure 1 as a green arrow. The black arrow (which is in part covered by a blue one in the figure) corresponds to the total momentum $\mathbf{p}$. Its length, $\|\mathbf{p}\|$, is the center–center distance. This interpretation is useful for drawing some conclusions about the energy transfer event. For instance, it will only be possible if one sphere is not totally inside the other and if the two spheres are not too far apart from each other, that is, if $(R_i-R_j)^2 < \|\mathbf{p}\|^2 < (R_i+R_j)^2$. In vector notation, Eqs. 5 and 6 become

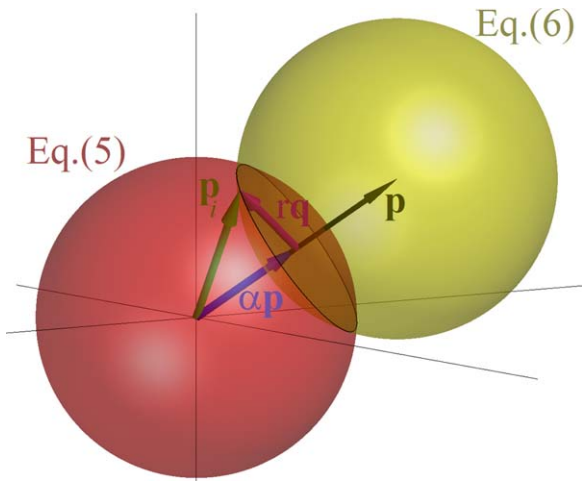

Figure 1. Geometric interpretation of the proposed algorithm.

The red spherical surface represents Eq. 5 and holds all possible momenta $\mathbf{p}_i$ after energy is transferred from particle *i* to particle *j*. The circumferential intersection between the red and yellow surfaces represents the solution of Eqs. 5 and 6, thus holding all momenta $\mathbf{p}_i$ that satisfy the conservation laws. Finally, the green arrow depicts the unique vector $\mathbf{p}_i=\alpha\mathbf{p}+r\mathbf{q}$ that satisfies the minimum disturbance criterion, with α, r, and $\mathbf{q}$ being calculated by Eqs. 11, 12, and 16, respectively. [Color figure can be viewed in the online issue, which is available at wileyonlinelibrary.com.]

$$\|\mathbf{p}_i\|^2=R_i^2 \quad \text{and} \tag{7}$$

$$\|\mathbf{p}_i-\mathbf{p}\|^2=\|\mathbf{p}_i\|^2-2\mathbf{p}\cdot\mathbf{p}_i+\|\mathbf{p}\|^2=R_j^2. \tag{8}$$

By substituting Eq. 7 into Eq. 8 and isolating the scalar product $\mathbf{p}\cdot\mathbf{p}_i$, we conclude that the intersection circumference lies in the plane defined by

$$\mathbf{p}\cdot\mathbf{p}_i=\frac{R_i^2+\|\mathbf{p}\|^2-R_j^2}{2} \tag{9}$$

The momentum $\mathbf{p}_i$ can be regarded as a vector sum $\mathbf{p}_i=\alpha\mathbf{p}+r\mathbf{q}$, where $\alpha\mathbf{p}$ and $r\mathbf{q}$ are two orthogonal vectors represented in Figure 1 by arrows colored in blue and in magenta, respectively. The vector $\alpha\mathbf{p}$ comes from the projection of $\mathbf{p}_i$ onto the direction of $\mathbf{p}$, that is

$$\alpha\mathbf{p}=\frac{\mathbf{p}\cdot\mathbf{p}_i}{\|\mathbf{p}\|}\frac{\mathbf{p}}{\|\mathbf{p}\|} \tag{10}$$

Thus, the constant α is equal to $\mathbf{p}\cdot\mathbf{p}_i/\|\mathbf{p}\|^2$. Applying Eq. 9, this constant can be readily calculated by

$$\alpha=\frac{R_i^2+\|\mathbf{p}\|^2-R_j^2}{2\|\mathbf{p}\|^2} \tag{11}$$

The terms that compose the other vector in the sum, $r\mathbf{q}$, are the radius r of the intersection circumference and a unity vector $\mathbf{q}$. As one can see in Figure 1, such radius is related to the lengths of $\alpha\mathbf{p}$ (blue arrow) and $\mathbf{p}_i$ (green arrow) by the Pythagorean theorem. Therefore, once α is evaluated, we can compute r by

$$r=\sqrt{R_i^2-\alpha^2\|\mathbf{p}\|^2} \tag{12}$$

Finally, it is necessary to determine $\mathbf{q}$. Although it has three components, this problem has a unique degree of freedom, as it is known that $\|\mathbf{q}\|=1$ (unitarity) and that $\mathbf{p}\cdot\mathbf{q}=0$ (orthogonality to $\mathbf{p}$). In other words, it is necessary to choose the point of the black circumference in Figure 1 to which the green arrow will be directed. The criterion defined for this choice is the key feature of the proposed method, which intends to exchange energy while causing the smallest possible disturbance to the system. A suitable measure for such disturbance is the square of the distance between the momentum of particle i before and after the energy transfer, that is

$$d^2=\|\alpha\mathbf{p}+r\mathbf{q}-\mathbf{p}_i^0\|^2=\|\alpha\mathbf{p}-\mathbf{p}_i^0\|^2-2r\mathbf{p}_i^0\cdot\mathbf{q}+r^2 \tag{13}$$

The only nonconstant term above is $-2r\mathbf{p}_i^0\cdot\mathbf{q}$, which means that we should look for the vector $\mathbf{q}$ that maximizes the scalar product $\mathbf{p}_i^0\cdot\mathbf{q}$, subject to the constraints $\|\mathbf{q}\|=\mathbf{q}\cdot\mathbf{q}=1$ and $\mathbf{p}\cdot\mathbf{q}=0$. By the method of Lagrange multipliers, we define a function $f(\mathbf{q})=\mathbf{p}_i^0\cdot\mathbf{q}+\Lambda_1(\mathbf{q}\cdot\mathbf{q}-1)+\lambda_2\mathbf{p}\cdot\mathbf{q}$ and make $\nabla_{\mathbf{q}}f=\mathbf{0}$, which gives

$$\mathbf{p}_i^0+2\Lambda_1\mathbf{q}+\Lambda_2\mathbf{p}=\mathbf{0} \tag{14}$$

Applying a scalar product with $\mathbf{p}$ to both sides of the equation above and given that $\mathbf{p}\cdot\mathbf{q}=0$, we obtain $\Lambda_2=-(\mathbf{p}\cdot\mathbf{p}_i^0)/\mathbf{p}\cdot\mathbf{p}$. Then, defining a vector $\mathbf{Q}=2\Lambda_1\mathbf{q}$, thus proportional to $\mathbf{q}$, we get

$$\mathbf{Q}=\mathbf{p}_i^0-\frac{\mathbf{p}\cdot\mathbf{p}_i^0}{\|\mathbf{p}\|^2}\mathbf{p} \tag{15}$$

Finally, as we know that $\mathbf{q}$ is unitary, the two possible options are $\pm\mathbf{Q}/\|\mathbf{Q}\|$. We must choose the one that maximizes $\mathbf{p}_i^0\cdot\mathbf{q}$, rather than minimizing it. The solution will be the one that makes such scalar product positive. Therefore

$$\mathbf{q}=\begin{cases}\mathbf{Q}/\|\mathbf{Q}\| & \text{if } \mathbf{p}_i^0\cdot\mathbf{Q}\geq 0\\ -\mathbf{Q}/\|\mathbf{Q}\| & \text{if } \mathbf{p}_i^0\cdot\mathbf{Q}<0\end{cases} \tag{16}$$

In summary, once the particles and the amount of energy to be transferred are chosen, Eqs. 11, 12, and 16 are evaluated and the new linear momenta are obtained as $\mathbf{p}_i=\alpha\mathbf{p}+r\mathbf{q}$ and $\mathbf{p}_j=\mathbf{p}-\mathbf{p}_i$, from which the corresponding velocities follow directly. This is a very simple algorithm which has the advantage of allowing energy to be exchanged between particles with different masses. Of course, an attempted transfer can be carried out only if the conditions $\Delta E\leq E_i^0$ and $(R_i-R_j)^2<\|\mathbf{p}\|^2<(R_i+R_j)^2$ are met. If they are not met, we simply abstain from transferring energy at that particular time step. This does not jeopardize the applicability of the method, but means that we cannot always predefine the long-term energy transfer rate as $\Delta E/\tau_{\text{exch}}$, where τ_{exch} is the interval between transfer attempts. Restrictions of this type simply reflect the physical limit to the amount of energy that can be transferred without violating the conservation laws. They are expected to exist in any algorithm that allows ΔE to be specified (see, e.g., Ref. 37). However, as shown in Results section, full acceptance is generally observed with the proposed algorithm, except in extreme cases when large energy fluxes are simulated with exceedingly high (i.e., way above optimal) values of τ_{exch}.

We note that the proposed algorithm is analogous to the nonisotropic velocity scaling (NIVS) method of Kuang and Gezelter,[37] but has two key distinctions that should be remarked. First, minimum disturbance is the main criterion of our method, used to choose the new momenta from a continuum of possibilities, while it is only a secondary criterion in the NIVS method. Second, our formulation is simpler and does not require solving a quartic equation at every transfer event, as NIVS does. Finally, we note that NIVS is originally formulated to involve all particles at the tagged slabs in the energy exchange, while our original formulation involves only a selected pair of particles. However, this not an actual distinction, as either method could be easily reformulated in the other way.

Methodology

Thermal conductivity

Besides the proposed algorithm, the methods of MP[19] and of ND&A[21] were used in this work to determine the thermal conductivity of the simulated systems. To perform a fair comparison of the algorithms, the same criterion was used to choose the particles that will exchange energy, which are the fastest atom in the cold slab and the slowest atom in the hot slab. It is important to note that transferring energy between single atoms is the worst case scenario for testing the energy drift problem, because the whole disturbance in each tagged slab is being localized rather than being spread throughout it.[38]

The steady-state energy flux across the system (J) and temperature at each slab k (T_k) are determined in the same way as in the MP and ND&A methods. Considering that the box was divided along the z axis and that the transient part of the simulation has been properly discarded, we have

$$J=\frac{\sum_{\text{transfers}}\Delta E}{2tL_xL_y} \text{ and} \tag{17}$$

$$T_k=\frac{1}{3n_kk_B}\left\langle\sum_{i\in k}^{n_k}m_i\|\mathbf{v}_i\|^2\right\rangle \tag{18}$$

where n_k is the number of atoms in slab k, $\mathbf{v}_i$ is the velocity of atom i, m_i is the mass of the same atom, t is the total steady-state simulation time, and L_x and L_y are the side lengths of the simulation box in the x and y directions, respectively. The angle brackets denote a time average taken along the simulated steady state.

Considering that a linear temperature profile is observed along the z direction, the thermal conductivity is calculated by

$$\lambda=\frac{J_z}{\partial T/\partial z} \tag{19}$$

where the gradient is estimated by linear regression.

Simulation details

All simulations were carried out using the open-source software LAMMPS,[45] whose code was modified to include

the algorithm proposed here. Periodic boundary conditions were considered and the Velocity-Verlet algorithm was employed to integrate the Newtonian equations of motion.[12] The time step size and the aspect of the simulation box will be defined on a case-by-case basis. Fixed NVE simulations were employed in all thermal conductivity determinations, but preliminary NVT and NPT simulations were useful for generating initial configurations and for determining the system density in each case. The force fields employed for *n*-octane were NERD[39] and a version of OPLS-UA,[40–42] modified to include harmonic bonds and angles. The parameters for bond stretching and angle bending were taken from the OPLS-AA force field.[41] The flexible SPC/Fw[43] force field was used to model water, and the Lennard-Jones potential was considered for argon with parameters $\varepsilon_b = 1$ kJ/mol and $\sigma = 0.3405$ nm.[46] The Lorentz-Berthelot mixing rule was employed for unlike interactions and Ewald summation[12,47] was used to evaluate long-range electrostatic interactions of water. The cutoff distances were 1.4 nm for *n*-octane, 0.9 nm for water, and 3σ for argon (standard long-range corrections[12] were used in all simulations).

Parameters for algorithm evaluation

The BD-NEMD algorithms used in this work were compared using molecules and force fields with different characteristics. The NERD force field was employed to test the proposed algorithm with molecules with relatively stretchy bonds while the modified OPLS force field presents stiffer bonds. Water with a flexible potential (SPC/Fw) was chosen to evaluate the algorithm with molecules that present electrostatic interactions. Finally, high-density argon was simulated to test the algorithms for systems without intramolecular degrees of freedom.

The energy drift and temperature variation were evaluated by computing the overall energy increase (ξ) and the overall temperature variation (ΔT) parameters during the simulation runs, which are defined as

$$\xi = \frac{\langle E_T \rangle_f - \langle E_T \rangle_0}{\langle E_T \rangle_0} \text{ and} \tag{20}$$

$$\Delta T = \langle T \rangle_f - \langle T \rangle_0 \tag{21}$$

where $\langle\,\rangle_0$ and $\langle\,\rangle_f$ denote averages taken for a number of steps at the beginning and at the end of the steady-state simulation, respectively, E_T is the total energy, and T is the average temperature of the simulation box.

As some conditions must be fulfilled at a given simulation step so that the proposed algorithm can actually perform the energy exchange, we report the ratio of successful exchanges (θ) using the equation

$$\theta = \frac{E_T^{exch}}{E_T^{max}} \times 100\% \tag{22}$$

where E_T^{exch} is the total energy exchanged during the simulation and $E_T^{\max}$ is the energy that would have been exchanged if all attempted transfers were successful.

The standard deviations of all results were determined using standard correlation analysis.[12] The reported uncertainty of every result is twice the corresponding standard deviation.

Density determination

The procedure for determining the density of *n*-octane was the same for both force fields employed. All simulations reported in this section were performed using a 1-fs time step. Initially, 400 *n*-octane molecules were packed into a cubic simulation box with periodic boundary conditions and an initial density around 280 kg/m^3 using the software Packmol.[53] To avoid local minimum trapping, a Nosé–Hoover chain thermostat with standard LAMMPS parameters was used to warm up the system from 300 to 700 K during 25 ps. After equilibration at this temperature for 2 ns, the system was cooled down to 300 K during 300 ps. Next, volume was allowed to vary by fixing the pressure at 1 atm using a Nosé–Hoover barostat, also with standard LAMMPS parameters. After another 2 ns equilibration, a production run of 10 ns was used to determine the density of *n*-octane.

For water, the procedure was the same, but with minimum and maximum temperatures equal to 323 and 450 K, respectively, initial density around 680 kg/m^3, and number of molecules equal to 500.

Initial configurations

Initial configurations were prepared in elongated boxes with $L_z = 3L_x = 3L_y$ for *n*-octane and argon, and with $L_z = 2L_x = 2L_y$ for water, considering the densities previously determined. The warming/cooling procedure was used once again to avoid local minima, followed by 2 ns NVT equilibration at the desired temperature using a Berendsen thermostat, and then a 5 ns equilibration with fixed NVE. Exceptionally, argon was equilibrated using the Berendsen thermostat at 83.7 K and 1428.3 kg/m^3 for 10^7 time steps, followed by an NVE equilibration with another 10^7 time steps. The final configurations obtained with the described procedure served as initial configurations for thermal conductivity determinations.

Nonequilibrium simulations

The simulation box was divided along the z axis into 20 slabs of equal thickness. Attempts of energy transfer between the fastest atom in the cold slab and the slowest atom in the hot slab were carried out at uniform intervals of time. Different energy exchange period τ_{exch} were used because it may affect the performance of BD-NEMD methods. For both methods ND&A and MP, τ_{exch} were 500 and 1000 fs for *n*-octane, 200 and 500 fs for water, and 10 and 50 time steps for argon. The energy flux observed in each condition using ND&A and MP methodologies were reproduced using the proposed algorithm using τ_{exch} values ranging from 1 fs to the maximum τ_{exch} used with ND&A and MP methods.

The simulations were carried out during 15 ns for *n*-octane and water and 5×10^6 time steps for argon. The first 1 ns for *n*-octane and water and the first 10^5 time steps for argon were taken to reach the steady state. The temperature in each slab was sampled at every 100 fs for *n*-octane and water and at every 200 time steps for argon.

Slabs where the exchange occurred were excluded of λ determination to enhance the statistical quality. The overall energy (ξ) and temperature variation (ΔT) were evaluated for each case studied here.

Results and Discussion

Density values determined as described in the previous section are shown in Table 1. The obtained densities showed good agreement with literature data, except for the modified OPLS force field. The values for *n*-octane were 1.43% below the reference data for the NERD force field and 5.44% above the reference data for the modified OPLS force field.

Table 1. Simulated Densities of *n*-Octane (300 K) and Water (323 K) Compared to Experimental Results

	ρ (kg m^{-3})	
Compound	This Work	Reference
n-Octane (NERD)	688	698[48]
n-Octane (OPLS-UA)	736	698[48]
Water (SPC/Fw)	1004	996[49]

The latter was not reparametrized after bond stretching and angle bending were taken into account, which may be the cause of the observed discrepancy. In view of this fact, the results obtained using this force field were used only for qualitative comparisons. In the case of water, the simulated density was 0.80% higher than the reference experimental value, which is in agreement with the findings reported in Ref. 43 for the SPF/Fw force field.

The conditions used in each BD-NEMD simulation were described in the preceding section. For convenience, we now introduce a notation that simplifies the comparison among different methods with distinct parameters. One must keep in mind that the exchange periods are always expressed in femtoseconds. For the MP or the ND&A algorithms, we use the letters MP or ND, respectively, followed by the employed exchange period. For instance, ND500 corresponds to the ND&A algorithm with an exchange period of 500 fs. For the proposed algorithm, we use the letters PA followed by the exchange period of a reference simulation (MP or ND&A) used to define the desired energy flux, followed by the actual exchange period employed in the method. For example, PA500-2 means that an actual exchange period of 2 fs was used to produce the same energy flux of a reference simulation whose exchange period was 500 fs.

n-Octane systems

Tables 2–4 show thermal conductivities obtained using the different methods and force fields, as well as the measured evaluation parameters: overall energy variation (ξ), overall temperature variation (ΔT), and percentage of successful exchanges (θ).

As observed in Table 2, in the case of the NERD force field the overall energy and temperature variations were reduced in more than 50% when PA500-2 was employed, when compared to ND500. For a smaller energy flux, PA1000-2 reduced the overall energy variation in 75% when compared to ND1000 and practically no temperature variation was observed. Note that an exchange period of 2 fs corresponds to performing exchanges at every time step. Table 3 contains results for the modified OPLS force field using a time step of 1 fs. As one can see, the behavior previously observed using NERD was not verified here when energy is exchanged at every time step. The reduction in the overall energy variation, when compared to the reference ND&A simulation, was about 10% only. For the modified OPLS force field using a 2 fs time step, whose results are shown in Table 4, the overall energy and temperature variation were the largest ones, considering all conditions evaluated for *n*-octane. First of all, this demonstrates that such a large time step size is unsuitable for systems involving chemical bonds that are so stiff. The bond force constants of OPLS are more than twice as large as the equivalent ones of NERD. These observations suggest that the energy drift problem is related to anomalous deformation of bond lengths and other geometric features (e.g., angles and dihedrals) of molecules that take part in energy exchange events.

Another observation is that about 40–45% of the energy transfer attempts were unsuccessful when high exchange periods were used in the proposed algorithm. Once the methodology is based on the intersection of spheres in the space of linear momenta, and the radii of these spheres depend on the amount of energy being transferred, the conditions

Table 2. Overall Energy Increase (ξ), Temperature Variation (ΔT), Percentage of Successful Exchanges (θ), and Thermal Conductivities (λ) of *n*-Octane Using NERD Force Field and Employing Different BD-NEMD Algorithms and EMD Simulation Method

Algorithm	λ (W/m K)	ξ' (%)	ΔT (K)	θ (%)
ND500	0.096 ± 0.001	3.59	3.61 ± 0.57	–
PA500-2	0.096 ± 0.001	1.70	1.47 ± 0.28	100.00
PA500-40	0.096 ± 0.001	4.53	4.58 ± 0.40	100.00
PA500-250	0.097 ± 0.001	4.57	4.40 ± 0.37	100.00
PA500-500	0.095 ± 0.001	1.59	1.84 ± 0.38	61.56
ND1000	0.093 ± 0.001	0.89	0.88 ± 0.43	–
PA1000-2	0.095 ± 0.001	0.23	0.00 ± 0.33	100.00
PA1000-40	0.095 ± 0.001	1.39	1.34 ± 0.30	100.00
PA1000-500	0.096 ± 0.001	1.30	1.00 ± 0.45	100.00
PA1000-1000	0.096 ± 0.002	0.34	0.50 ± 0.48	54.88
Reference	0.130[50]			

Table 3. Overall Energy Increase (ξ), Temperature Variation (ΔT), Percentage of Successful Exchanges (θ), and Thermal Conductivities (λ) of *n*-Octane Using the Augmented OPLS-UA Force Field with 1-fs Time Step and Employing Different BD-NEMD Algorithms and EMD Simulation Method

Algorithm	λ (W/m K)	ξ' (%)	ΔT (K)	θ (%)
ND500	0.070 ± 0.000	9.43	5.09 ± 0.47	–
PA500-1	0.071 ± 0.000	8.59	4.58 ± 0.49	100.00
PA500-40	0.071 ± 0.000	11.22	6.32 ± 0.48	100.00
PA500-250	0.073 ± 0.000	10.40	5.53 ± 0.45	100.00
PA500-500	0.068 ± 0.000	4.95	3.01 ± 0.30	63.36
ND1000	0.065 ± 0.001	3.88	2.00 ± 0.45	–
PA1000-1	0.062 ± 0.001	3.46	1.73 ± 0.38	100.00
PA1000-40	0.063 ± 0.001	5.07	2.86 ± 0.36	100.00
PA1000-500	0.064 ± 0.001	4.56	2.34 ± 0.27	100.00
PA1000-1000	0.064 ± 0.001	1.66	0.75 ± 0.51	56.81
Reference	0.130[50]			

Table 4. Overall Energy Increase (ξ), Temperature Variation (ΔT), Percentage of Successful Exchanges (θ), and Thermal Conductivities (λ) of *n*-Octane Using the Augmented OPLS-UA Force Field with 2-fs Time Step and Employing Different BD-NEMD Algorithms and EMD Simulation Method

Algorithm	λ (W/m K)	ξ' (%)	ΔT (K)	θ (%)
ND500	0.074 ± 0.001	38.79	21.95 ± 0.42	–
PA500-2	0.071 ± 0.001	41.36	23.25 ± 0.61	100.00
PA500-40	0.074 ± 0.001	46.69	26.35 ± 0.70	100.00
PA500-250	0.074 ± 0.001	43.21	24.17 ± 0.72	100.00
PA500-500	0.068 ± 0.001	19.78	11.34 ± 0.34	58.70
ND1000	0.064 ± 0.001	16.14	9.05 ± 0.62	–
PA1000-2	0.064 ± 0.001	16.29	9.30 ± 0.57	100.00
PA1000-40	0.066 ± 0.001	20.04	11.32 ± 0.34	100.00
PA1000-500	0.067 ± 0.001	18.32	10.29 ± 0.50	100.00
PA1000-1000	0.061 ± 0.001	6.85	3.74 ± 0.46	55.03
Reference	0.130[50]			

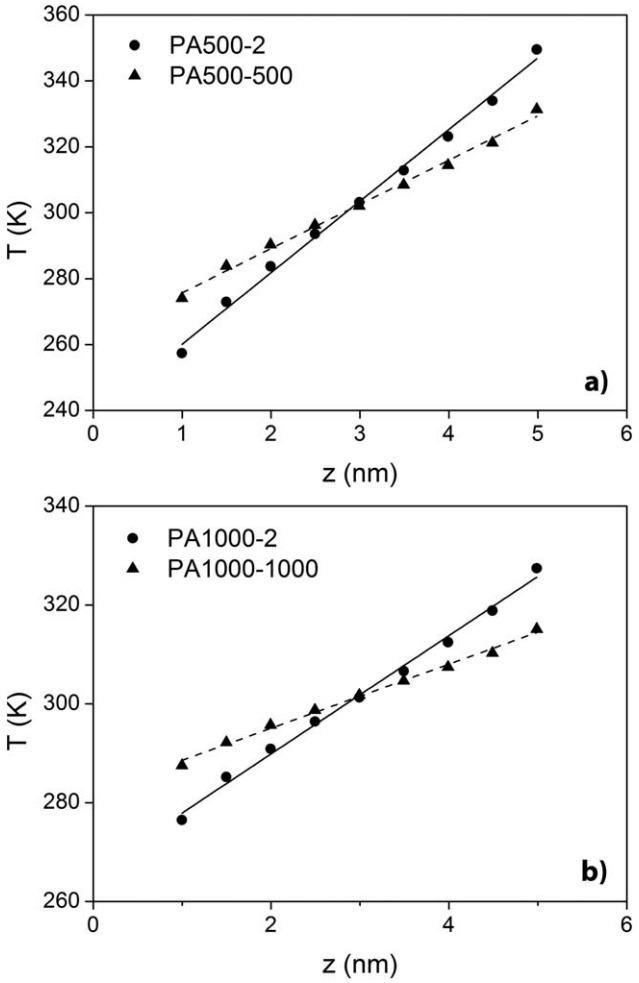

Figure 2. Temperature profiles for *n*-octane modeled with the NERD force field.

(a) Energy exchange periods of 500 fs or equivalent. (b) Energy exchange periods of 1000 fs or equivalent.

needed for intersections to exist are often unfulfilled when a large amount of energy is to be transferred in a single step. Nevertheless, the overall energy drift and temperature variation observed in these cases were the smallest ones. This can be explained by the fact that, due to the rate of unsuccessful attempts, the simulation did not achieve the desired heat flux. As a consequence, the resulting temperature gradient was smaller than the ones observed in other cases and, therefore, the reduction in the energy drift cannot be considered as a real gain in this case.

This leads to the conclusion that the proposed algorithm had its best performance when a small amount of energy was exchanged at every time step.

Following the work of Zhang et al.,[35] we examined the density and temperature profiles along the z direction of the simulation box. In all cases, statistically equivalent slabs were averaged and the profiles were fitted by linear regression. The temperatures in all slabs were between 40 K above the melting point and 40 K below the boiling point of *n*-octane. Figure 2 contains the temperature profiles for *n*-octane modeled with the NERD force field which presented the smallest energy drift. The density profile for *n*-octane using the proposed algorithm with an exchange period of 2 fs and NERD force field is shown in Figure 3. All the obtained density profiles of *n*-octane were similar and exhibited liquid-like behavior in the whole domain. The temperature profiles presented linear behavior for all cases, with coefficients of determination (R^2) higher than 0.994, ensuring that the systems were in the linear regime.

Thermal conductivity values determined with different algorithms agree, which demonstrates the validity of the proposed methodology. The simulated results were about 25% smaller than the experimental results, in the case of the NERD force field. Other authors reported deviations of similar magnitudes.[39] The analysis of evaluation parameters obtained for *n*-octane suggests that the proposed algorithm may drastically reduce the energy drift when applied to molecules with soft bond interactions, but the reduction is less pronounced if the molecules present large force constants controlling their internal degrees of freedom.

Water systems

Systems containing 812 water molecules were simulated to investigate the behavior of the proposed algorithm when electrostatic interactions are present. Two energy exchange schemes were considered in this case. In the first scheme, any atom (either oxygen or hydrogen) was allowed to exchange energy with any other atom. In the second scheme, only oxygen atoms were allowed to participate in the exchange events. To evaluate the proposed algorithm with respect to the energy drift problem, the ND&A algorithm was used as a reference for the first scheme, while the MP algorithm served as a reference for the second one.

The determined thermal conductivities and evaluation parameters for all water systems are shown on Tables 5 and 6. Note that the proposed algorithm has a bad performance related to the energy drift when energy transfers involve atoms with large differences in mass (Table 5). As the algorithm operates by transferring fixed amounts of energy, light atoms like hydrogen might accelerate or slow down too much as a result of a transfer event, thus revealing a considerable perturbation to the system dynamics. This effect is magnified when large exchange periods are employed, similarly to what occurred in the *n*-octane simulations, but it is also noticeable when a small energy amount is exchanged at every time step. Although the disturbance on the atom

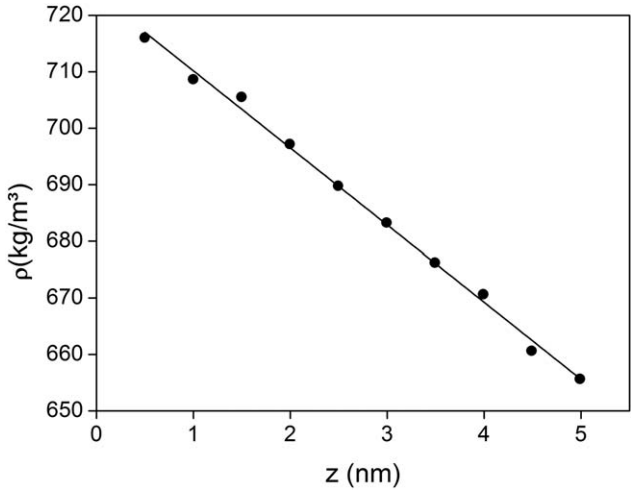

Figure 3. Density profile of *n*-octane modeled with the NERD force field and an energy exchange condition of PA200-2.

Table 5. Overall Energy Increase (ξ), Temperature Variation (ΔT), Percentage of Successful Exchanges (θ), and Thermal Conductivities (λ) of Water Using the SPC/Fw Force Field and Employing Different BD-NEMD Algorithms Performing Energy Exchanges Between All Types of Atoms

Algorithm	λ (W/m K)	ξ' (%)	ΔT (K)	θ (%)
ND200	0.708 ± 0.012	-6.68	18.03 ± 0.31	–
PA200-1	0.774 ± 0.014	-7.71	20.50 ± 0.35	100.00
PA200-20	0.766 ± 0.020	-12.64	34.14 ± 0.43	100.00
PA200-100	0.692 ± 0.016	-5.29	14.39 ± 0.31	57.85
PA200-200	0.710 ± 0.017	-4.30	11.34 ± 0.30	54.45
ND500	0.707 ± 0.020	-2.45	6.05 ± 0.31	–
PA500-1	0.792 ± 0.025	-2.85	7.90 ± 0.27	100.00
PA500-20	0.797 ± 0.033	-5.96	16.19 ± 0.28	100.00
PA500-250	0.730 ± 0.036	-2.53	6.43 ± 0.27	58.35
PA500-500	0.712 ± 0.036	-1.62	4.43 ± 0.33	54.56
Reference	0.618[51]			

velocities is small at every event, the number of non-Newtonian integration steps becomes large and more than compensates such positive effect. Another point that must be addressed is the way of choosing the atoms that will exchange energy. As we always choose the fastest atom at the cold slab and the slowest atom at the hot slab, it is possible that the same atoms keep being chosen at successive steps, which might also have an effect on the energy and temperature variations observed.

The considerations above are reinforced by the results obtained with transfers being allowed solely between oxygen atoms, as one can see in Table 6. The smallest energy variation occurred when the proposed algorithm was used with exchange periods of 20 fs, independently of the heat flux. The PA500-20 condition presented a reduction of more than 80% on the energy drift when compared to MP500. According to Raabe and Sadus,[52] the period of vibration of the oxygen-hydrogen bond in water is around 13 fs. Therefore, 20 fs seems to be enough for the exchanged energy to spread among adjacent atoms, thus allowing the molecule to relax. In addition, performing transfers at every time step for a system presenting electrostatic interactions seems to increase the round-off and cutoff noises so that they noticeably contribute to the overall energy variation. Nevertheless, it has been shown that the algorithm proposed here can be used to reduce the energy drift issue in systems with electrostatic interactions.

The temperature profiles for some simulated water systems are shown in Figure 4. The density profile was also evaluated for water to confirm the liquid-like behavior over the entire domain and is shown in Figure 5 for the MP200 condition (which is similar to the results at all other conditions). All the obtained temperature profiles were linear, showing

Table 6. Overall Energy Increase (ξ), Temperature Variation (ΔT), Percentage of Successful Exchanges (θ), and Thermal Conductivities (λ) of Water Using the SPC/Fw Force Field and Employing Different BD-NEMD Algorithms Performing Energy Exchanges Between Oxygen Atoms

Algorithm	λ (W/m K)	ξ' (%)	ΔT (K)	θ (%)
MP200	1.003 ± 0.012	-0.65	1.95 ± 0.23	–
PA200-1	1.110 ± 0.051	21.38	-57.40 ± 0.63	100.00
PA200-20	1.014 ± 0.012	0.50	-1.44 ± 0.23	100.00
PA200-100	1.029 ± 0.013	-0.72	2.15 ± 0.21	96.13
PA200-200	0.998 ± 0.026	-0.37	1.24 ± 0.23	46.73
MP500	0.986 ± 0.028	-0.45	1.42 ± 0.31	–
PA500-1	1.043 ± 0.040	5.18	-13.67 ± 0.28	100.00
PA500-20	1.028 ± 0.030	-0.08	-0.17 ± 0.24	100.00
PA500-250	0.983 ± 0.028	-0.38	0.64 ± 0.27	99.87
PA500-500	1.119 ± 0.078	-0.14	0.29 ± 0.31	46.16
Reference	0.618[51]			

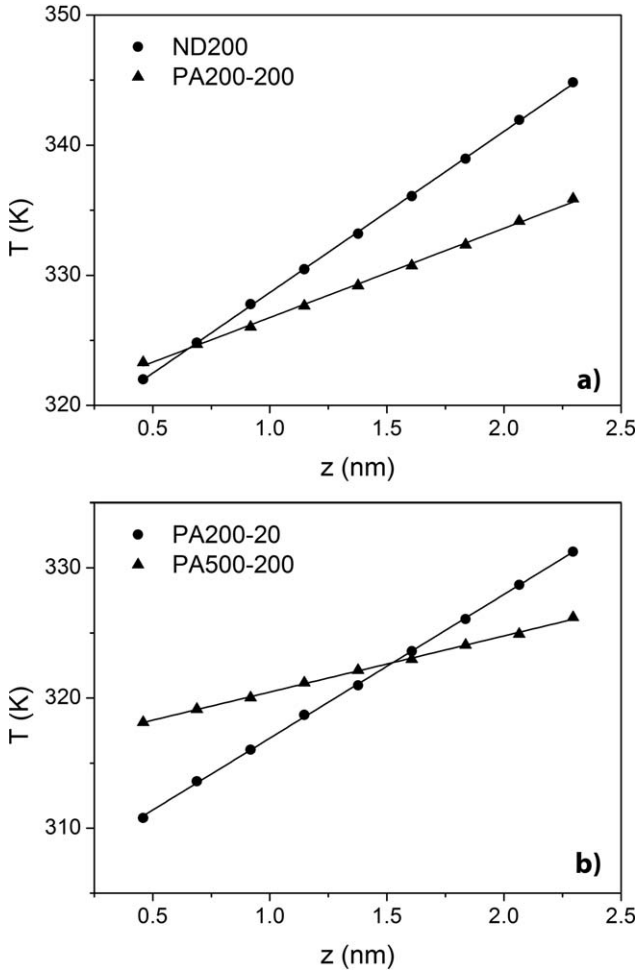

Figure 4. Temperature profiles for water modeled with the SPF/Fw force field.

(a) Energy exchanges using hydrogen and oxygen atoms. (b) Energy exchanges using only oxygen atoms.

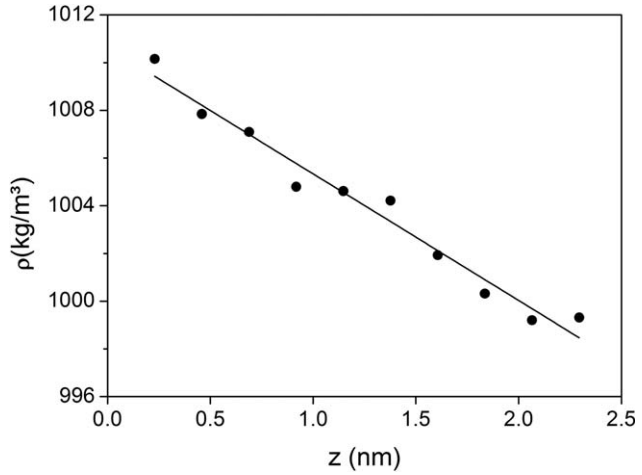

Figure 5. Density profiles for SPF/Fw water using the MP algorithm with energy exchange periods equal to 200 fs.

Table 7. Overall Energy Increase (ξ), Temperature Variation (ΔT), Percentage of Successful Exchanges (θ), and Thermal Conductivities (λ) of LJ Argon Employing Different BD-NEMD Algorithms

Algorithm	λ (W/m K)	ξ' (%)	ΔT (K)	θ (%)
MP10	0.127 ± 0.000	5.83	-2.58 ± 1.38	–
PA10-1	0.127 ± 0.000	5.48	-1.69 ± 1.16	100.00
PA10-2	0.131 ± 0.000	5.03	-1.84 ± 1.16	100.00
PA10-5	0.130 ± 0.000	4.49	-1.18 ± 1.00	100.00
PA10-10	0.133 ± 0.000	1.66	-3.90 ± 0.30	60.50
MP50	0.133 ± 0.001	0.28	-0.61 ± 0.12	–
PA50-1	0.131 ± 0.001	0.22	-0.50 ± 0.10	100.00
PA50-2	0.134 ± 0.001	0.22	-0.50 ± 0.13	100.00
PA50-25	0.133 ± 0.001	0.25	-0.52 ± 0.25	100.00
PA50-50	0.133 ± 0.001	0.05	-0.08 ± 0.11	52.71
Reference	0.132[51] ($T^* = 0.70$, $\rho^* = 0.84$)			

coefficients of determination at least equal to 0.998, ensuring that the system is in the linear regime. The highest and lowest temperatures were far from the freezing and boiling points of water in almost all cases, ensuring the absence of phase transitions. The only exception was the proposed algorithm with an exchange period of 1 fs, which approached the freezing point in the cold slab.

The thermal conductivity values determined with all BD-NEMD algorithms showed reasonable agreement with literature values, even when high energy variation occurred by doing exchanges between atoms of distinct masses. The values obtained with the proposed algorithm agreed with those obtained with other algorithms, with the advantage of presenting considerably smaller energy drift in some cases.

Argon systems

To evaluate how the energy variation takes place in systems without internal degrees of freedom, a system containing 3000 argon atoms next to the triple point was simulated (density equal to 1428.3 kg/m^3 and temperature equal to 83.7 K).

The overall energy variation, temperature variation, thermal conductivity, and percent ratio of successful energy exchanges are shown in Table 7. The proposed algorithm showed that the energy drift could be reduced up to 20% when compared to MP algorithm. The values of overall energy variation determined with different exchange periods for argon showed a different behavior when compared to water and *n*-octane studied here. While water and *n*-octane presented a point of maximum in ξ, the argon showed a continuously reduce in ξ with an increase energy exchange period. This observation reinforces the connection between the energy increase and the stretching of the molecular bonds and angles.

The determined thermal conductivity of argon using different algorithms showed a good agreement with literature data. The proposed algorithm showed a reduction in ξ from 6 to 83% when compared to MP algorithm. The deviations between simulation and literature data were all lesser than 4%, also confirming that the proposed algorithm predicts reliable thermal conductivity values with lesser energy drifts.

Conclusions

A new low-disturbance energy exchange BD-NEMD algorithm was proposed to generate thermal gradients in molecular dynamics simulations while the total energy and momentum are kept constants. This algorithm provides thermal conductivities (λ) resulting from simulations with smaller energy drift and temperature variation issues when compared to other PeX algorithms.

For the systems considered here, the proposed algorithm was tested in worst-case scenarios in terms of simulation conditions (i.e., conditions that would cause the highest energy drifts). Because the energy transfers were performed between atoms with the highest velocity difference (in magnitude), we expect high disturbances. Furthermore, the kinetic energy exchanges were carried out between single atoms instead of whole molecules. Nevertheless, the energy drifts were reduced up to 80%, reducing the need of coupling a thermostat to the systems. The proposed algorithm might be advantageous for systems that require long simulations.

The thermal conductivities obtained for water, octane, and argon agreed with those from literature and with values obtained from other well-known algorithms.

Acknowledgments

It is a pleasure to be part of this issue in honor of professor J. M. Prausnitz. By means of his books, especially Molecular Thermodynamics of Fluid-Phase Equilibria, he has enormous influence on our chemical engineering careers. In addition, F.W.T. had the chance to spend a sabbatical year at Berkeley with Prausnitz. In F.W.T.'s own words: "During this year, I benefited from talking and learning about not only science, but also history of science, American history, music, and art. I also visited, by his advising, several nice places in California, such as Point Lobos and Lake Tahoe. John's wisdom, enthusiasm, and humanistic vision touched me deeply and I am happy to have this opportunity to express my gratitude." The authors gratefully acknowledge the financial support of Petrobras (project code CENPES 16113) and the Brazilian agencies CNPq (Conselho Nacional de Desenvolvimento Científico e Tecnológico), CAPES (Coordenação de Aperfeiçoamento de Pessoal de Nível Superior), and FAPERJ (Fundação Carlos Chagas Filho de Amparo à Pesquisa do Estado do Rio de Janeiro).

Literature Cited

1. Warrier PW, Yuan Y, Beck MP, Teja AS. Heat transfer in nanoparticle suspensions: modeling the thermal conductivity of nanofluids. *AIChE J*. 2010;56:3243–3256.
2. Kruesi M, Jovanovic ZR, Haselbacher A, Steinfeld A. Analysis of solar-driven gasification of biochar trickling through an interconnected porous structure. *AIChE J*. 2014;61:867–879.
3. Aimoli CG, Maginn EJ, Abreu CRA. Transport properties of carbon dioxide and methane from molecular dynamics simulations. *J Chem Phys*. 2014;141:134101.
4. Ghorayeb K, Anraku T, Firoozabadi A. Interpretation of the fluid distribution and GOR behavior in the Yufutsu fractured gas-condensate field. In: Asia Pacific Conference on Integrated Modelling for Asset Management, Yokohama, Japan. SPE. 2000:SPE-59437-MS.
5. Montel F, Bickert J, Lagisquet A, Galliero G. Initial state of petroleum reservoirs: a comprehensive approach. *J Petrol Sci Eng*. 2007; 58:391–402.
6. Nikpoor MH, Kharrat R, Chen Z. Modeling of compositional grading and plus fraction properties changes with depth in petroleum reservoirs. *Petrol Sci Technol*. 2011;29:914–923.
7. Galliero G, Montel F. Understanding compositional grading in petroleum reservoirs thanks to molecular simulations. In: EUROPEC/EAGE Conference and Exhibition, Amsterdan, The Netherlands. SPE. 2009:SPE-121902-MS.

8. Janca J, Kaspárková V, Halabalová V, Simek L, Ruzcka J, Barosová E. Micro-thermal field-flow fractionation of bacteria. *J Chromatogr B*. 2007;852:512–518.
9. Firouzi M, Wilcox J. Molecular modeling of carbon dioxide transport and storage in porous carbon-based materials. *Microporous Mesoporous Mater*. 2012;158:195–203.
10. Kolditz O, Bauer S, Böttcher N, Elsworth D, Görke U-J, McDermott C-I, Park C-H, Singh AK, Taron J, Wang W. Numerical simulation of two-phase flow in deformable porous media: application to carbon dioxide storage in the subsurface. *Math Comput Simul*. 2012;82:1919–1935.
11. Das DB, Gill BS, Abidoye LK, Khudaida KJ. A numerical study of dynamic capillary pressure effect for supercritical carbon dioxide-water flow in porous domain. *AIChE J*. 2014;60:4266–4278.
12. Allen MP, Tildesley DJ. *Computer Simulation of Liquids*. New York: Oxford University Press, 1989.
13. Celik FA. Molecular dynamics simulation of polyhedron analysis of Cu–Ag alloy under rapid quenching conditions. *Phys Lett A*. 2014; 378:2151–2156.
14. Dysthe DK, Fuchs AH, Rousseau B. Prediction of fluid mixture transport properties by molecular dynamics. *Int J Thermophys*. 1998; 19:437–448.
15. Fernández GA, Vrabec J, Hasse H. A molecular simulation study of shear and bulk viscosity and thermal conductivity of simple real fluids. *Fluid Phase Equilib*. 2004;221:157–163.
16. Liang Z, Tsai H. Molecular dynamics simulations of self-diffusion coefficient and thermal conductivity of methane at low and moderate densities. *Fluid Phase Equilib*. 2010;297:40–45.
17. Evans DJ, Morriss GP. *Statistical Mechanics of Nonequilibrium Liquids*. London: Academic Press, 1990.
18. Hafskjold B, Tamio I, Ratkje SK. On the molecular mechanism of thermal diffusion in liquids. *Mol Phys*. 1993;80:1389–1412.
19. Müller-Plathe F. A simple nonequilibrium molecular dynamics method for calculating the thermal conductivity. *J Chem Phys*. 1997; 106:6082–6085.
20. Bedrov D, Smith GD. Thermal conductivity of molecular fluids from molecular dynamics simulations: application of a new imposed-flux method. *J Chem Phys*. 2000;113:8080–8084.
21. Nieto-Draghi C, Avalos JB. Non-equilibrium momentum exchange algorithm for molecular dynamics simulation of heat flow in multicomponent systems. *Mol Phys*. 2003;101:2303–2307.
22. Lervik A, Bresme F, Kjelstrup S. Heat transfer in soft nanoscale interfaces: the influence of interface curvature. *Soft Matter*. 2009;5:2407–2414.
23. Hulse RJ, Rowley RL, Wilding WV. Transient nonequilibrium molecular dynamic simulations of thermal conductivity: 1. Simple fluids. *Int J Thermophys*. 2005;26:1–12.
24. Thomas JC, Rowley RL. Transient molecular dynamics simulations of liquid viscosity for nonpolar and polar fluids. *J Chem Phys*. 2011; 134:24526–1–24526-9.
25. McQuarrie D. *Statistical Mechanics*. New York: Harper & Row, 1976.
26. Frenkel D, Smit B. *The Art of Molecular Simulation: From Algorithms to Applications*, *2nd ed*. San Diego, CA: Academic Press, 2002.
27. Rapaport DC. *The Art of Molecular Dynamics Simulation*, *2nd ed*. New York: Cambridge University Press, 2004.
28. Green MS. Markoff random processes and the statistical mechanics of time dependent phenomena. II. Irreversible processes in fluids. *J Chem Phys*. 1954;22:398–413.
29. Kubo R. Statistical-mechanical theory of irreversible processes. I. General theory and simple applications to magnetic and conduction problems. *J Phys Soc Jpn*. 1957;12:570–586.
30. Hoheisel C. *Transport Properties of Fluids: Their Correlation, Prediction and Estimation*. In: Millat J, Dymond JH, Nieto de Castro CA, editors. New York: Cambridge University Press, 1996.
31. Dysthe DK, Fuchs AH, Rousseau B. Fluid transport properties by equilibrium molecular dynamics. I. Methodology at extreme fluid states. *J Chem Phys*. 1999;110:4047–4059.
32. Reith D, Müller-Plathe F. On the nature of thermal diffusion in binary Lennard-Jones liquids. *J Chem Phys*. 2000;112:2436–2443.
33. Artola P-A, Rousseau B. Thermal diffusion in simple liquid mixtures: what have we learnt from molecular dynamics simulations? *Mol Phys*. 2013;111:3394–3403.
34. Zhang M, Müller-Plathe F. Reverse nonequilibrium molecular-dynamics calculation of the Soret coefficient in liquid benzene/cyclohexane mixtures. *J Chem Phys*. 2005;123:124502–1–124502-8.
35. Zhang M, Lussetti E, Souza LES, Müller-Plathe F. Thermal conductivities of molecular liquids by reverse nonequilibrium molecular dynamics. *J Phys Chem B*. 2005;109:15060–15067.
36. Zhang M. Thermal diffusion in liquid mixtures and polymer solutions by molecular dynamics simulations. Dr. rer. nat. Dissertation. Darmstadt: Technischen Universität Darmstadt, 2006.
37. Kuang S, Gezelter JD. A gentler approach to RNEMD: non isotropic velocity scaling for computing thermal conductivity and shear viscosity. *J Chem Phys*. 2010;133:164101-1–164101-9.
38. Kuang S, Gezelter JD. Velocity shearing and scaling RNEMD: a minimally perturbing method for simulating temperature and momentum gradients. *Mol Phys*. 2012;110:691–701.
39. Nath SK, Escobedo FA, Pablo JJ. On the simulation of vapor-liquid equilibria for alkanes. *J Chem Phys*. 1998;108:9905–9911.
40. Jorgensen WL, Madura JD, Swenson CJ. Optimized intermolecular potential functions for liquid hydrocarbons. *J Am Chem Soc*. 1984; 106:6638–6646.
41. Jorgensen WJ, Maxwell DS, Tirado-Rives J. Development and testing of the OPLS all-atom force field on conformational energetics and properties of organic liquids. *J Am Chem Soc*. 1996;118:11225–11236.
42. Huang DM, Sendner C, Horinek D, Netz RR, Bocquet L. Water slippage versus contact angle: a quasiuniversal relationship. *Phys Rev Lett*. 2008;101:226101–1–226101-4.
43. Wu Y, Tepper HL, Voth GA. Flexible simple point-charge water model with improved liquid-state properties. *J Chem Phys*. 2006; 124:024503-1-024503-12.
44. Müller-Plathe F, Bordat P. Reverse non-equilibrium molecular dynamics. In: Karttunen M, Vattulainen I, Lukkarinen A, editors. *Novel Methods in Soft Matter Simulations, Lecture Notes in Physics, Vol. 640*. Berlin Heidelberg: Springer-Verlag, 2004:310–326.
45. Plimpton S. Fast parallel algorithms for short-range molecular dynamics. *J Comput Phys*. 1995;117:1–19.
46. Michels A, Wijker H, Wijker HK. Isotherms of argon between 0°C and 150°C and pressures up to 2900 atmospheres. *Physica*. 1949;15: 627–633.
47. Ewald PP. Die Berechnung optischer und elektrostatischer Gitterpotentiale. *Ann Phys*. 1921;369:253–287.
48. Dreisbach RR. *Physical Properties of Chemical Compounds II*. Washington: American Chemical Society, 1959.
49. Perry RH, Green DW. *Perry's Chemical Engineers' Handbook*, 7th ed. New York: McGrawHill, 1997.
50. Yaws CL. *Transport Properties of Chemicals and Hydrocarbons: Viscosity, Thermal Conductivity, and Diffusivity of C1 to C100 Organics and Ac to Zr Inorganics*, *1st ed*. New York: William Andrew Inc., 2009.
51. David RL. *CRC Handbook of Chemistry and Physics*, 90th ed. Boca Raton, FL: CRC Press, Taylor and Francis, 2010.
52. Raabe G, Sadus RJ. Molecular dynamics simulation of the effect of bond flexibility on the transport properties of water. *J Chem Phys*. 2012;137:104512–1–104512-8.
53. Martínez L, Andrade R, Birgin EG, Martínez JM. Packmol: a package for building initial configurations for molecular dynamics simulations. *J Comput Chem*. 2009;30:2157–2164.

Manuscript received Dec. 19, 2014, and revision received Mar. 10, 2015.